Carbohydrate Polymers 229 (2020) 115458

Contents lists available at ScienceDirect

Carbohydrate Polymers

journal homepage: www.elsevier.com/locate/carbpol

Macroporous methacrylated hyaluronic acid cryogels of high mechanical strength and flow-dependent viscoelasticity

Burak Tavsanli, Oguz Okay*

Department of Chemistry, Istanbul Technical University, 34469 Maslak, Istanbul, Turkey

ARTICLE INFO

Keywords:
Hyaluronic acid
Cryogels
Macroporous
Viscoelasticity
Mechanical properties

ABSTRACT

We present here a new approach for the fabrication of macroporous hyaluronic acid (HA) cryogels with a tunable porous structure, flow-dependent viscoelasticity, and a high mechanical strength. They were synthesized from methacrylated HA in aqueous solutions at −18 °C by free-radical mechanism using in situ prepared poly(*N, N*-dimethylacrylamide) (PDMAA) as a spacer. Both the porosity and the average diameter of the pores decrease from 99 to 90% and from 150 to 90 μm, respectively, with increasing PDMAA content of the cryogels due to the simultaneous decrease in the amount of ice template during cryogelation. The cryogels also exhibit reversible strain-dependent apparent gel-to-sol transition due to the flowing-out and flowing-in water through the pores. This flow-dependent viscoelasticity is of great interest as it protects HA network from damage under large strain and hence acts as a self-defense mechanism.

1. Introduction

Hyaluronic acid (HA), a significant component of the extracellular matrix, is a high-molecular weight natural polysaccharide with a large water holding capacity due to its polyelectrolyte nature (Fraser, Laurent, & Laurent, 1997). Although HA attracts significant interest over many years in soft tissue regeneration due to its excellent lubricating, self-healing, and biological functions (Chen & Abatangelo, 1999; Zamboni, Viera, Reis, Oliveira, & Collins, 2018), easy degradability and weak mechanical behavior of HA limit its application areas (Collins & Birkinshaw, 2008; Valachova et al., 2016). To overcome these limitations, hydrogels based on native or chemically modified HA have been reported (Collins & Birkinshaw, 2008; Leach, Bivens, Patrick, & Schmidt, 2003; Prado, Weaver, & Love, 2011; Tavsanli, Can, & Okay, 2015). Several cross-linkers including ethylene glycol diglycidyl ether (EGDE), glutaraldehyde, and divinyl sulfone have been used in the preparation of HA hydrogels (Collins & Birkinshaw, 2007, 2013; Horkay, Hecht, & Geissler, 2006; Hwang et al., 2012; Kim et al., 2012; Segura et al., 2005; Tomihata & Ikada, 1977). Alternatively, HA was first modified to incorporate methacrylate groups to enable cross-linking, and then polymerized to form HA hydrogels (Ibrahim, Kothapalli, Kang, & Ramamurthi, 2011; Leach et al., 2003; Prado et al., 2011). It was shown that the hydrogels based on both native and methacrylated HA exhibit a good biocompatibility as well as a slow rate of degradation as compared to the native uncross-linked HA (Weng, Gouldstone, Wu, & Chen, 2008). However, these hydrogels are generally brittle in nature because of the lack of an effective energy dissipation in the covalently cross-linked HA network (Ahagon & Gent, 1975; Brown, 2007).

Recently, we have shown that an improvement in the mechanical properties of HA hydrogels could be achieved when silk fibroin is incorporated into the HA network that forms β-sheet crystallites acting as physical cross-links (Tavsanli & Okay, 2019). Another strategy is double- or triple-networking of HA hydrogels with ductile network components based on poly(*N,N*-dimethylacrylamide) (PDMAA) (Tavsanli et al., 2015; Weng et al., 2008), a non-cytotoxic polymer for various applications interfacing with biological systems such as in medicine (Babic et al., 2009; Li et al., 2011; Wang, Yong, Deng, & Wu, 2018; de Queiroz, Castro, & Higa, 1997; Abraham, de Queiroz, & Roman, 2001). Although a mechanical property improvement in the resulting double- or triple-network HA hydrogels could be achieved, this multi-step synthetic procedure is lengthy and complicated.

Cryogelation is a simple and versatile technique for the fabrication of macroporous hydrogels, also called cryogels (Lozinsky & Okay, 2014; Lozinsky, 2002; Okay & Lozinsky, 2014). It is also more environmentally friendly as compared to alternative techniques because water is generally used as the solvent, and there is no need to use organic solvents as porogens. The principle of this technique is to carry out the cross-linking reactions of linear polymers in aqueous solutions below their freezing points. As water freezes, polymer chains rejected

* Corresponding author.
E-mail address: okayo@itu.edu.tr (O. Okay).

https://doi.org/10.1016/j.carbpol.2019.115458
Received 6 September 2019; Received in revised form 26 September 2019; Accepted 7 October 2019
Available online 15 October 2019
0144-8617/

from the ice and concentrated in the unfrozen regions result in the formation of a highly concentrated solution phase, called cryoconcentration. Thus, cryogelation system at thermal equilibrium with the surrounding is composed of a concentrated polymer-cross-linker solution together with the ice template distributed along the system (Okay & Lozinsky, 2014). Cryogelation leads to the formation of cross-linked polymers even at very low polymer concentrations due to the fact that the effect of the cryoconcentration commonly dominates over the reduction in the cross-linking rates at low temperatures. After cryogelation and melting of ice temple, a 3D polymer network containing macropores is obtained.

Physically cross-linked HA cryogels exhibiting a storage modulus of around 100 Pa were prepared via freeze-thaw induced gelation at a low pH (Cai, Zhang, Wei, & Zhang, 2017). HA cryogels sustaining up to around 30 kPa compressive stresses have also been prepared in an aqueous NaOH solution (pH > 10) of HA at −18 °C using EGDE as a chemical cross-linker (Strom, Larsson, & Okay, 2015). However, the selection of a NaOH solution as the solvent to conduct the cross-linking reactions is not appropriate as it promotes the degradation of HA (Oelschlaeger, Bossler, & Willenbacher, 2016; Tavsanli & Okay, 2016). It seems challenging to produce macroporous HA hydrogels and scaffolds with appropriate mechanical properties to closely mimic mechanical properties of the extracellular matrix, structural stability, and an effective mechanism of energy dissipation under strain.

We present here a new cryogelation approach for the fabrication of macroporous HA cryogels with a wide variety of properties, flow-dependent viscoelasticity (poroelasticity), complete squeezability, and a high mechanical strength. HA cryogels were synthesized from methacrylated HA of varying methacrylation degree in aqueous solutions at −18 °C by free-radical mechanism using a redox initiator system. Our preliminary experiments showed that methacrylated HA alone could not form water-insoluble cryogels likely due to the steric effect of HA molecules. However, incorporation of a small amount of a vinyl monomer such as *N, N*-dimethylacrylamide (DMAA) in the feed resulted in a complete gelation at −18 °C. This reveals spacer effect of PDMAA chains interconnecting HA units, as illustrated in Scheme 1. As will be seen below, HA cryogels in swollen state sustain up to 2.6 ± 0.2 MPa compressive stress, which is around 2 orders of magnitude higher than those obtained by EGDE cross-linker (Strom et al., 2015). HA cryogels confined between parallel plates also exhibit reversible strain-dependent apparent gel-to-sol transition behavior due to the flowing-out and flowing-in water through the pores, similar to water squeezing out of a sponge. This flow-dependent viscoelasticity of HA cryogels, known as poroelasticity (Hu & Suo, 2012; Nosellia, Lucantonioa, McMeeking, & DeSimonea, 2016; Oyen, 2014), is similar to that observed with articular cartilage (Lu & Mow, 2008), a low-friction and load bearing soft tissue, providing the joint with vital biomechanical functions, such as wear resistance, load bearing, and shock absorption for around a century. Under compression, the liquid within the cartilage flows out of the tissue through the pores, as observed in HA cryogels, which produces high frictional resistance and hence frictional energy dissipation responsible for the viscoelastic behavior of articular cartilage (Lu & Mow, 2008). Gel-to-sol transition behavior of HA cryogels presented here is also of great interest in biomaterial and biomedical applications as it protects HA network from damage under large strain conditions and hence acts as a self-defense mechanism.

2. Experimental section

2.1. Materials

The sodium salt of hyaluronic acid from *Streptococcus equi* (HA) with a viscosity average molecular weight of $\sim 1.2 \times 10^6$ g·mol^{-1} (Strom et al., 2015), glycidyl methacrylate (GM), *N,N*-dimethylacrylamide (DMAA), tetrabutylammonium bromide (TBAB), ammonium persulfate (APS), *N,N,N',N'*-tetramethylethylenediamine (TEMED), all from Sigma-Aldrich, triethylamine (TEA, Merck), and acetone (Tekkim, Turkey), were used as received. A stock solution of APS was prepared by pipetting 10 mL distilled water onto 0.8 g APS and dissolving at 23 ± 2 °C. HA was methacrylated following a protocol by Leach et al. (2003). In short, 0.5 g of HA was added into 50 mL distilled water and stirred overnight for complete dissolution. GM (1 mL), TEA (1 mL), and TBAB (1 g) were then dissolved in this HA solution to obtain a GM / disaccharide repeat unit molar ratio of 6. After the reaction at 55 °C, the solution was precipitated in an excess of acetone and dissolved in distilled water twice. The solution of methacrylated HA (meth-HA) was then freeze-dried for 2 days. Fourier transform infrared (FTIR) spectroscopy was used to demonstrate the incorporation of methacrylate groups onto the HA backbone (Figure S1a). The methacrylation degree of meth-HA was determined from nuclear magnetic resonance (NMR) spectra recorded on a 500 MHz Agilent VNMR spectrometer, as reported before (Leach et al., 2003; Tavsanli et al., 2015) (Figure S1b).

2.2. Preparation of cryogels

Methacrylated HA (meth-HA) with methacrylation degrees of 4, 14, and 25% was used in the synthesis of the cryogels. In our experiments, the concentration of meth-HA was set to 1 wt % whereas DMAA concentration was varied between 0.5 and 5 wt %. Typically, to prepare cryogels at 1 wt % DMAA, meth-HA (0.100 g) was added into 9.8 mL distilled water and gently stirred overnight for complete dissolution. DMAA (0.100 g) was then dissolved in this solution under stirring for 30 min. After cooling the solution to 4 °C under bubbling nitrogen to prevent gelation before freezing at −18 °C, TEMED (25 μL) and APS stock solution (0.1 ml) were added. The solution was then poured into 1-mL plastic syringes and cylindrical glass vials of 4.6 and 40 mm in

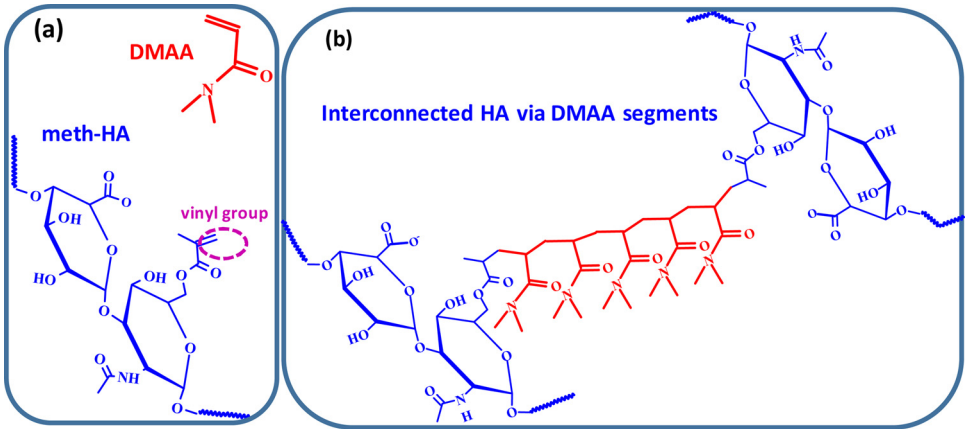

Scheme 1. DMAA and repeat unit of methacrylated HA (meth-HA, blue) before (a) and after interconnecting with DMAA segments (red). Note that the reaction between glycidyl methacrylate and HA to form meth-HA proceeds via transesterification and ring opening routes (Leach et al., 2003; Tavsanli et al., 2015). For the sake of clarity, the chemical structure of meth-HA formed by the former route is shown in (a).

internal diameters, respectively, that were immersed in a deep freezer at −18 °C and the cryogelation reactions were conducted for 5 days.

2.3. Quantifying the amount of unfrozen water during cryogelation

Differential scanning calorimetry (DSC) was used to estimate the unfrozen water content and the true monomer concentration during cryogelation. Reaction solutions with 1 wt % meth-HA and various amounts of DMAA were first prepared without addition of the initiator system to avoid gelation. Meth-HA/DMAA solutions were then poured into plastic syringes that were placed in a deep freezer at −18 °C for 24 h. Frozen specimens weighing approximately 20 mg were placed into the DSC pans of Perkin-Elmer Diamond DSC instrument which were then sealed and weighed. Each pan was cooled in the DSC to −18 °C, held at this temperature for 2 h, and then heated to 30 °C at a rate of 1 °C min^{-1}. The mass fraction f_{unf} of water remaining unfrozen in meth-HA/DMAA solution at −18 °C was calculated as

$$f_{unf} = 1 - \frac{\Delta H}{\Delta H_m} \quad (1)$$

where ΔH and ΔH_m are the melting enthalpies of frozen water in the specimen in kJ mol^{-1}, and of ice (6.01 kJ mol^{-1}), respectively.

2.4. Characterization of HA cryogels

The measurements of the swelling degrees and gel fractions were performed by immersing the cryogel specimens of about 1 cm in length in an excess of water at 23 ± 2 °C for 1 week to remove soluble species, followed by freeze-drying (Christ Alpha 2e4 LD-plus) for 2 days. The gel fraction W_g, that is the mass of water-insoluble HA-DMAA network obtained from one gram of meth-HA and DMAA was calculated as

$$W_g = \frac{m_{dry}}{m_o\, C_o} \quad (2)$$

where m_{dry} and m_0 represent the masses of the specimens in freeze-dried state and just after preparation, respectively, C_o is the concentration of meth-HA and DMAA in the initial reaction solution. The equilibrium swelling ratios of HA cryogels in water by weight q_w and volume q_v were calculated as

$$q_w = \frac{m_s}{m_{dry}} \quad (3)$$

$$q_v = \left(\frac{D_s}{D_{dry}}\right)^3 \quad (4)$$

where m_{dry} and D_{dry} are the mass and the diameter of freeze-dried samples, respectively, and m_s and D_s are the same quantities for samples in their equilibrium swollen states in water.

Rheological measurements were carried out on a Gemini 150 rheometer system (Bohlin Instruments) equipped with 40 mm parallel plates, a solvent trap filled with water to avoid water evaporation, and a Peltier device for temperature control. The gap distance was set to 800–1200 μm depending on the sample thickness. The measurements were conducted on the cryogels prepared in cylindrical glass vials of 40 mm in internal diameter that were cut into 1.0 ± 0.2 mm slices with a razor blade. The angular frequency ω dependences of the storage G' and loss moduli G'' of the cryogels were determined at a fixed strain γ_o of 1% which was within the linear viscoelastic range of HA cryogels.

The porous structure HA scaffolds was investigated using scanning electron microscopy (SEM) measurements conducted on a Tescan GAIA 3 Field Emission SEM. The measurements were performed on freeze-dried gel specimens after sputter-coating with gold-palladium on a Leica ACE 600 instrument. The average diameter D of the pores was calculated using ImageJ image processing software (NIH) with data from 50 pores of at least 10 SEM images of different magnification. The porous morphology of freeze-dried HA scaffolds was also studied using micro-computed tomography (μ-CT) scanning conducted on a μ-CT Skyscan 1272 instrument (Skyscan, Bruker, Belgium), as detailed before (Su & Okay, 2019). The following parameters were used: Voltage = 55 kV, current = 60 μA, pixel resolution = 8 μm, integration time = 70 ms.

Mechanical compression tests were conducted at 23 ± 2 °C on a Zwick Roell instrument using 500 N load cell. An initial compressive force of 0.01 N was applied before the tests to ensure a complete contact between the specimen and the plates. Cubic gel specimens with dimensions 3 × 3 x 3 mm were used for the measurements. The tests were carried out at 0.3 and 1 mm·min^{-1} strain rates below and above 15% compression, respectively. The nominal stress σ_{nom} which is the force per cross-sectional area of undeformed specimen and the fractional deformation ε were recorded. Young's modulus E was calculated from the 5–15% strain region in the stress–strain curves. The compressive strength and compression at break were estimated from the maxima of true stress–strain curves (Argun, Can, Altun, & Okay, 2014) (for details, see the Supporting Information text and Figure S2).

The swelling ratios, gel fractions, and mechanical data reported here are averages of experiments performed at least in duplicate. They all are collected in Table S1 and expressed as means ± SD.

3. Results and discussion

Hyaluronic acid (HA) cryogels were fabricated from methacrylated HA (meth-HA) in aqueous solutions at −18 °C using APS-TEMED redox initiator system. Meth-HA with 3 different methacrylation degrees, namely 4, 14, and 25% was used at a fixed concentration of 1 wt %. Because HA and its disaccharide repeating units have molecular weights of 1.2 × 10^6 and 416.2 g mol^{-1}, respectively, increasing the degree of methacrylation from 4 to 25% also increases the average number of pendant vinyl groups per HA chain from 115 to 720 and hence, increases its cross-linking functionality. Preliminary experiments conducted at various subzero temperatures and initiator concentrations showed no gel formation when meth-HA was used alone in the cryogelation, which we attribute to the steric hindrance of HA molecules restricting the cross-linking reactions. However, incorporation of a small amount of a spacer such as *N, N*-dimethylacrylamide (DMAA) into the monomer feed resulted in complete gelation. It is likely that meth-HA acts as a multifunctional macro-cross-linker during the free-radical polymerization of DMAA (Scheme 1). We selected DMAA for the present research because poly(DMAA) (PDMAA) is a biocompatible polymer with several attractive properties (Babic et al., 2009; Li et al., 2011; Wang et al., 2018; Weng et al., 2008; de Queiroz et al., 1997; Abraham et al., 2001; Uzumcu, Guney, & Okay, 2018; Uemura, McNulty, & Macdonald, 1995). Moreover, previous work shows that the redox-initiated polymerization of DMAA without a chemical cross-linker in a moderately frozen aqueous medium leads to the formation of water-insoluble cryogels (Zaborina, Gasanov, Peregudov, & Lozinsky, 2014). Although the cross-link density of the resulting cryogels is low, the self-cross-linking ability of DMAA may further contribute to the elasticity of the present HA cryogels. To highlight the effect of DMAA on the cryogel properties, its concentration in the reaction solution was varied from 0.5 up to 5 wt %, above which no gel could be obtained.

3.1. Swelling behavior, squeezability, and flow-dependent viscoelasticity

After the cryogelation reactions, the reaction components meth-HA and DMAA were completely incorporated into the cryogel network, as evidenced by the gel fraction tests (Table S1). Fig. 1a shows the equilibrium weight q_w (filled symbols) and volume swelling ratios q_v (open symbols) of HA cryogels with various DMAA contents in water as a function of the methacrylation degree (Meth) of HA. HA cryogels have a large degree of swelling by weight q_w varying between 22 and 140, that decreases with increasing DMAA content or Meth of HA. In contrast, the swelling ratio by volume q_v is 20- to 100-times smaller than q_w and

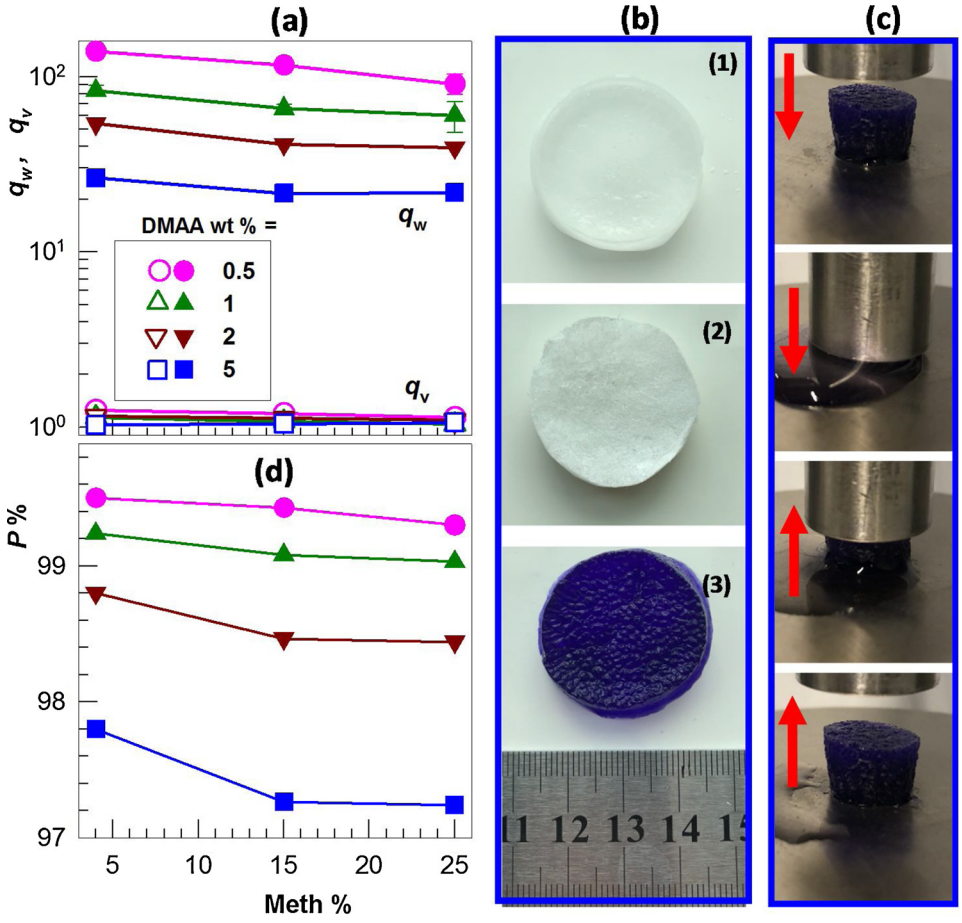

Fig. 1. (a): Equilibrium weight q_w (filled symbols) and volume swelling ratios q_v (open symbols) of HA cryogels in water shown as a function of the methacrylation degree (Meth) of HA. DMAA contents are indicated. Most of the error bars showing standard deviations of experiments performed at least duplicate are smaller than the size of the symbols. **(b):** Cryogel images after preparation (1), after freeze-drying (2), and after swelling equilibrium in water that was colored before with crystal violet. DMAA = 5 wt %. Meth = 25%. **(c):** Cryogel images under loading up to 90% strain and then unloading, indicated by down and up arrows, respectively. DMAA = 5 wt %. Meth = 25%. **(d):** Porosity P of the cryogels plotted against Meth %. Symbol explanations are displayed in Fig. 1a.

almost independent of DMAA content and methacrylation degree of HA (Table S1, Figure S3). For instance, Fig. 1b shows images of a cryogel specimen formed at 5 wt % DMAA and 25% Meth after preparation (image 1), after freeze-drying (image 2), and after swelling equilibrium in water colored with a dye (image 3). Although the volume change of the cryogel is negligible after swelling (q_v = 1.06 ± 0.02), its mass 22-fold increases after swelling suggesting filling of the micro-voids in the cryogel with water without changing its volume. This is an indirect indication of the existence of a 3D open pore structure in HA cryogels, as will be detailed in the next section.

Another feature of water-swollen HA cryogels is that they can almost completely and reversibly be squeezed under force without any damage. This behavior is illustrated in Fig. 1c showing the images of a swollen cryogel specimen in water colored with crystal violet. Compressing the specimen under load up to 90% strain squeezes out water from the cryogel network (down arrows in the images), whereas upon unloading, water released from the network is sucked back immediately and hence, the specimen autonomously recovers its original shape (up arrows). These cycles composed of squeezing followed by autonomic reswelling steps could be repeated 20 times without a change in the weight swelling ratio q_w of the cryogels and it remained at 22 ± 2. In contrast to HA cryogels, the corresponding HA hydrogels prepared at 23 ± 2 °C were not squeezable and they all fractured at around 60% compression (Figure S4).

To measure the fatigue resistance properties of the cryogels, they were subjected to cyclic compression tests at a constant strain rate of 1 mm·min^{-1}. The samples were first compressed up to a maximum strain of 90% and then unloaded to zero strain. This loading-unloading cycle was repeated 20 times with a waiting time of 1 min between the cycles. It was found that each loading or unloading curve follows the previous one indicating that the cycles are reversible and the cryogels are self-recoverable (Figure S5). Indeed, the area between the loading and unloading curves, i.e., the hysteresis energy U_{hys} is almost independent on the number of cycles and equals to 2.1 ± 0.3 kJ·m^{-3} (Figure S5). Because U_{hys} is the dissipated energy during the cyclic loading (Tuncaboylu, Sahin, Argun, Oppermann, & Okay, 2012), this indicates recovery of the virgin microstructure of the cryogels during the wait time between the cycles. Thus, self-recoverability of the cryogels reveals a high fatigue resistance against successive loadings.

Squeezability of HA cryogels as demonstrated in Fig. 1c reveals reversible flow-out and flow-in of water through the pores under high and low strain, respectively. Thus, if the strain is applied to a cryogel specimen confined between the parallel plates of a rheometer, one may expect that the flow-out water will surround the specimen providing its liquid-like response to the stress whereas upon reducing the applied strain, flow-in water will recover its gel-like response (Yetiskin & Okay, 2019). In order to verify this for HA cryogels, cyclic strain-sweep tests were carried out between 1 and 1000% strains (γ_o) at a fixed frequency ω of 6.3 rad s^{-1}. Fig. 2 shows γ_o-dependent variations of the storage modulus G' (filled symbols), loss modulus G'' (open symbols), and the loss factor $tan\ \delta$ (= G''/G', lines) of a cryogel specimen formed at 5 wt % DMAA and 25% Meth. Results of up and down strain sweep tests are shown by circles and triangles, respectively. It is seen that G'' starts to dominate over G', i.e., an apparent gel-to-sol transition takes place at ~20% strain above which the cryogel behaves as a low density liquid. The cryogel regain its initial viscoelastic properties after reducing the strain back to 1%, revealing the reversibility of the solid to liquid-like transition (Fig. 2). Similar results were also observed for all cryogels formed at various DMAA contents and Meth %. This behavior thus verifies the effect of flowing-out and flowing-in water on the viscoelastic response of the cryogels. It is worth to mention that this gel-to-sol transition is only an apparent transition because the gel network

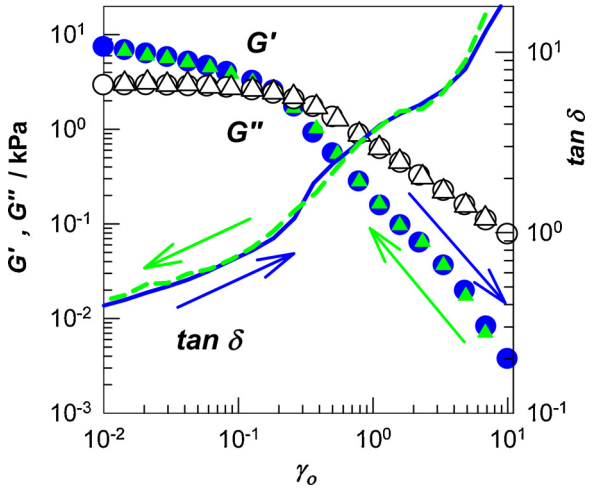

Fig. 2. Storage modulus *G'* (filled symbols), loss modulus *G"* (open symbols), and loss factor *tan δ* of a cryogel specimen formed at 5 wt % DMAA and 25% Meth as a function of strain γ_o. $\omega = 6.3$ rad·s^{-1}. Dynamic moduli data of up and down strain sweep tests are shown by the circles and triangles, while tan *δ* data are shown by the solid and dashed lines, respectively. Temperature = 25 °C.

remains intact under strain while the rheometer measures the response of the flowing-out water surrounding the gel. The observed poroelastic behavior associated with the flowing-out and flowing-in water is similar to that of articular cartilage, as detailed in the introduction (Lu & Mow, 2008; Malandrino & Moeendarbary, 2019; Mow, Kuei, Lai, & Armstrong, 1980; Soltz & Ateshian, 1998). This behavior is also of great interest in biomaterial and biomedical applications as it protects the HA network from damage under large strain conditions and hence increases its lifetime.

3.2. Porous structure and cryoconcentration effect

Because swelling of a cross-linked HA by volume results in the expansion of HA network in water due to the attractive HA–water interactions, while swelling by weight additionally involves pore filling with water and thereby mass increase, one may estimate the total open porosity *P* from the difference between q_w and q_v by,

$$P\,\% = \left(1 - \frac{q_v}{1 + (q_w - 1)\,d_2/d_1}\right) x\,10^2 \quad (5)$$

where d_1 and d_2 are densities of water (1.0 g·mL^{-1}) and HA/PDMAA (1.8 g·mL^{-1}), respectively (Okay, 2000). Fig. 1d showing the Meth-dependence of *P* reveals that all cryogels have 97–99% porosities. The lower the DMAA content or the methacrylation degree of HA, the higher is the porosity of the cryogels and it becomes 99.5% at 0.5 wt % DMAA and 4% Meth (Table S1). The porous structure of the cryogels was investigated using destructive SEM and nondestructive μ-CT techniques. SEM provides a higher magnification and thus a greater accuracy in the size determination of the pores than μ-CT. We have to note that all the samples were freeze-dried before subjecting to SEM and μ-CT measurements. Although the cryogels exhibit a high weight-swelling ratio due to the filling of the pores with water, their volume swelling ratios are close to unity, 1.11 ± 0.07 (Table S1), revealing that they do not expand or shrink significantly during swelling or freeze-drying, respectively. Therefore, the change in the porous morphology after freeze-drying is expected to be negligible. Figs. 3a, b show typical 2D and 3D μ-CT images of the cryogels synthesized at 1 and 5 wt % DMAA, respectively, and at a fixed methacrylation degree of 14%. HA cryogel with 1 wt % DMAA has a larger pore area (black) as compared to that with 5 wt % DMAA, which is in accord with Fig. 1d. Moreover, no noticeable effect of Meth on the porous structure of the cryogels was observed from 2D and 3D μ-CT images (Figure S6). An important requirement for macroporous polymers in many application areas is the presence of interconnecting pores. μ-CT showed the absence of closed pores in all samples and thus, the cryogels have an interconnected open pore structure.

Fig. 4 presents typical SEM images of HA cryogels prepared at DMAA contents between 0.5 and 5 wt % as indicated. Scale bars are 500 and 200 μm in the upper and bottom panel, respectively. The structure consists of μm-sized irregular pores whose sizes decrease while the pore walls become thicker as the DMAA content is increased. Similar to μ-CT results, no effect of Meth on the porous structure of the cryogels was observable from the SEM images. Fig. 3c shows the pore diameters estimated by analyzing μ-CT and SEM images of the cryogels prepared at various DMAA contents. We have to note that, because the pixel resolution of μ-CT is 8 μm, the precision in estimating the pore diameters using μ-CT is lower than that of SEM. Above 0.5 wt % DMAA, both images give similar diameters *D*, e.g., it decreases from around 150 to 90 μm as DMAA content is increased from 0.5 to 5 wt %. Simultaneously, the total porosity decreases from 94 to 88% whereas the thickness of the pore walls increases from 17 to 23 μm. At the lowest DMAA content of 0.5 wt %, SEM images show existence of 182 ± 42 μm pores in diameter whereas μ-CT analysis gives polydisperse pores of 147 ± 138 μm in diameter together with large pores of around 0.7 mm forming 11% of the total pore volume. It is likely that some of the pores collapse during drying due to the low polymer content of the cryogels formed at 0.5 wt % DMAA.

The results thus reveal decreasing porosity and average pore diameter with increasing amount of DMAA during cryogelation. The experimental findings can be explained with the actual concentrations of meth-HA and DMAA in the unfrozen regions as well as the total volume of ice during cryogelation. To determine these parameters, we performed DSC analysis on reaction mixtures which were thermally equilibrated at −18 °C. Fig. 5a shows DSC scans from -18 to 30 °C of the mixtures containing 1 wt % meth-HA and various amounts of DMAA. The endothermic melting peak moves to lower temperatures and the peak area becomes smaller with increasing amount of DMAA wt %, indicating decreasing the melting temperature T_m and the amount of ice at −18 °C. For instance, T_m calculated from the onset temperature decreases from -1.9 to -8.5 °C as DMAA content is increased from 0.5 to 10 wt % DMAA. Fig. 5b shows the fraction f_{unf} of unfrozen water during cryogelation at −18 °C as a function of DMAA wt %. f_{unf} is around 4% at 0.5 wt % DMAA, i.e., 96% of water is frozen during cryogelation and hence, acts as a template, whereas f_{unf} rapidly increases and becomes 17 ± 3% at 5 wt % DMAA. Further increase of DMAA content to 10 wt % results in 46 ± 6% unfrozen water. As mentioned above, no gelation was observed at DMAA contents above 5 wt %.

The true concentrations C_{true} of meth-HA and DMAA in the unfrozen regions, and the ice volume V_{ice} per gram dry cryogel were estimated using the equations,

$$C_{true} = \frac{10^2 C_{nom}}{C_{nom} + (1 - C_{nom}) f_{unf}} \quad (6)$$

$$V_{ice} = \frac{(1 - C_{nom})(1 - f_{unf})}{d_1 C_{nom}} \quad (7)$$

where d_1 is the ice density at −18 °C (0.995 g mL^{-1}), and C_{nom} is the nominal concentration, which is 1 wt % for meth-HA and 0.5–10 wt. % for DMAA. In Fig. 5c, the concentration ratio C_{true}/C_{nom} (circles) and the ice volume V_{ice} (triangles) are shown as a function of DMAA wt %. It is seen that the lower the DMAA concentration, the higher is the C_{true}/C_{nom} ratio, i.e, the extent of cryoconcentration. For instance, at 0.5 wt % DMAA, the C_{true}/C_{nom} ratio is around 22 indicating 22-fold increase of DMAA concentration under cryogelation condition as compared to the initial concentration. Increasing DMAA content decreases the cryoconcentration effect and the C_{true}/C_o ratio reduces to 4.4 and 2 at 5

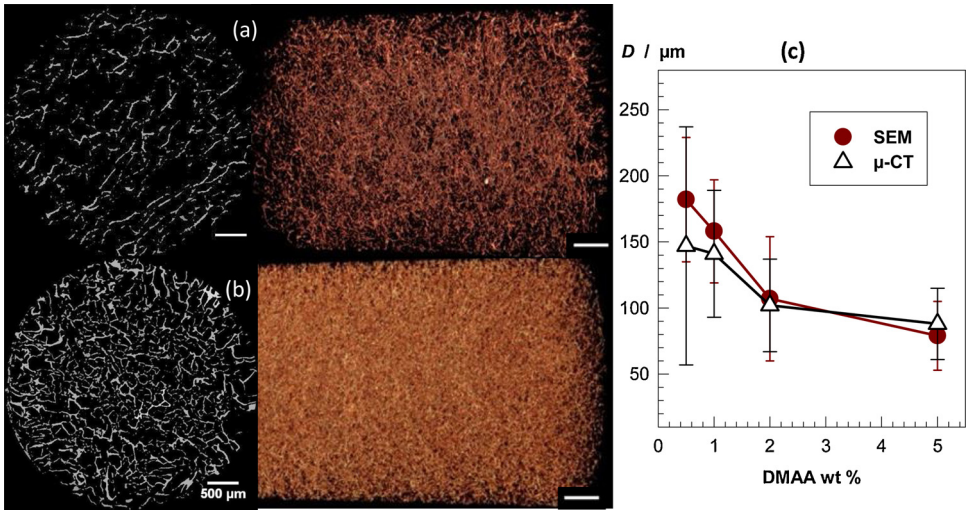

Fig. 3. (a, b): 2D and 3D μ-CT images of HA cryogels synthesized at 1 (a) and 5 wt % DMAA (b). Scale bars are 0.5 mm. Meth = 14%. **(c):** Average pore diameter *D* of HA cryogels estimated from μ-CT (open triangles) and SEM (filled circles) plotted against DMAA wt %. Meth = 4%.

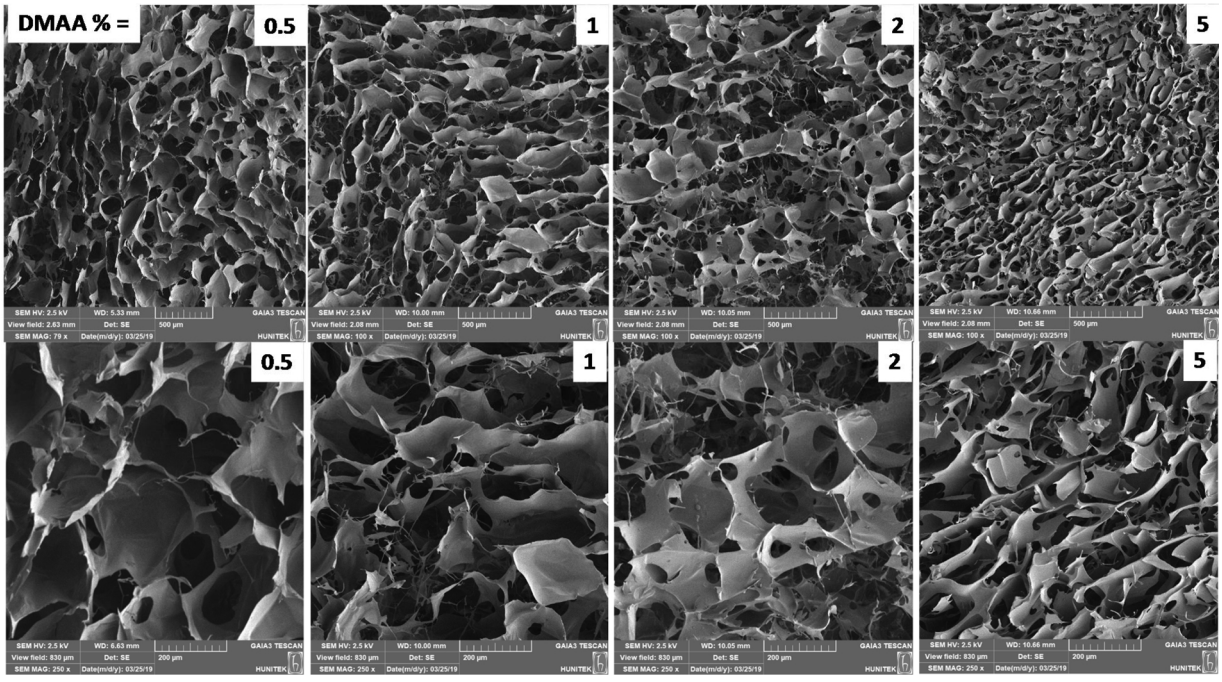

Fig. 4. SEM images of HA cryogels prepared at different amounts of DMAA. Scaling bars are 500 (top row) and 200 μm (bottom row). Meth = 4%.

and 10 wt % DMAA, respectively. This means that the true concentration C_{true} approaches to a limiting value of 20 wt % at $C_o \geq 5$ wt % revealing formation of a saturated meth-HA solution that remains unfrozen at −18 °C. The fact that no cryogel could be obtained above 5 wt % DMAA can thus be explained with decreasing extent of cryoconcentration. Thus, at high DMAA contents, reduced polymerization rates at −18 °C dominates over the cryoconcentration effect hindering the occurrence of the polymerization reactions of DMAA. Fig. 5c presenting the ice volume V_{ice} in the cryogels reveals continuous decrease of V_{ice} with increasing DMAA% which is due to simultaneous decreasing water content and in accord with the experimental results.

3.3. Viscoelastic and mechanical properties

Viscoelastic nature of HA cryogels was studied by rheological measurements at a strain γ_o of 0.01, which is in the linear viscoelastic region for all cryogels. Figs. 6a shows frequency ω dependences of the storage modulus *G'* and loss factor *tan δ* of HA cryogels prepared at a methacrylation degree of 4% and at various DMAA contents as indicated. Both *G'* and *tan δ* are nearly independent of the frequency ω below 1 rad·s^{-1} whereas frequency dependencies appear with increasing ω for high DMAA content. The storage modulus increases with increasing DMA wt % or methacrylation degree Meth of HA, reflecting increasing effective cross-link density of the cryogels (Fig. 6b). For instance, at Meth = 25%, *G'* measured at ω = 0.63 rad·s^{-1} increases from 0.6 to 5.5 kPa with increased DMAA content from 0.5 to 5 wt %. Moreover, the loss factor *tan δ* is above 0.1 for all cryogels which is typical for gels with a large extent of energy dissipation under force. This energy dissipation can be attributed to the flowing-out and flowing-in water through the porous network under a pressure gradient due to applied strain, producing frictional resistance and hence frictional energy dissipation, as discussed above (Fig. 2).

Mechanical properties of HA cryogels were investigated by uniaxial compression tests in their freeze-dried and swollen states at 23 ± 2 °C.

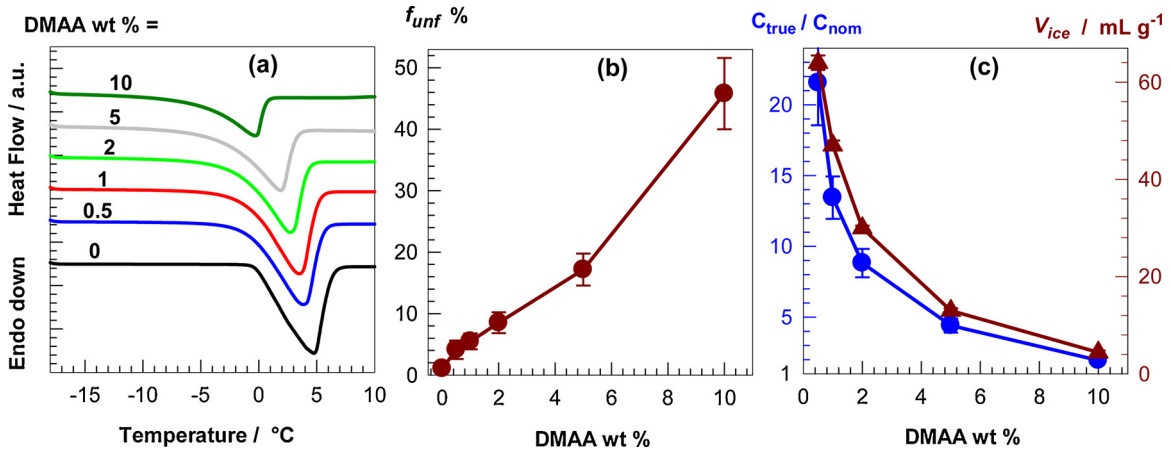

Fig. 5. (a): DSC scans of frozen meth-HA/DMAA solutions at various DMAA concentrations as indicated. Meth-HA = 1 wt %. Heating rate = 1 °C min^{-1}. **(b):** The fraction f_{unf} of unfrozen water at −18 °C shown as a function of DMAA wt %. **(c):** The concentration ratio C_{true} / C_{nom} (circles) and ice volume V_{ice} (triangles) shown as a function of DMAA wt %.

Fig. 7a, b show typical stress-strain curves of freeze-dried (a) and swollen cryogels (b) prepared at 4% Meth and various DMAA concentrations as indicated in the figures. To highlight the low strain region, the same curves over the whole range of strain are given in the insets in a semi-logarithmic scale. The stress-strain curves of dry cryogels are initially quite linear indicating elastic behavior but then, they exhibit a near-plateau regime where the samples are easily compressed. Finally, a steep increase in stress at strains above 80% is observed. The existence of a plateau regime in the stress-strain curves of dry cryogels indicates disruption of the pore structure in the cryogel networks. Thus, the steep increase in stress in the last region of the stress-strain curves reveals vanishing of the pores and thus, non-porous HA network is compressed in this region. The plateau stress increases with increasing DMAA wt % suggesting that the pore walls forming the 3D network structure become mechanically stronger at high DMAA contents. For example, it increases by one-order of magnitude with increasing DMAA content from 0.5 to 5 w/v %. In contrast, cryogels in swollen state exhibit no plateau region and very low modulus *E*, which is in the same range of that reported before for EGDE-cross-linked cryogels (Oelschlaeger et al., 2016; Strom et al., 2015). We attribute the disappearance of the plateau regime and the lowering modulus to the squeezability of the cryogels under strain (Fig. 1c).

Moreover, the stress-strain curves of swollen cryogels up to around 80% strain follow a similar path to those reported before for EGDE-cross-linked cryogels (Strom et al., 2015). However, the latter cryogels rupture above 80% strain whereas our cryogels sustain up to around 99% strain. The stability of the present cryogels under large strain conditions indicate their high toughness due to the energy dissipation mechanism created in the gel network. For instance, the area under the curve up to the fracture point corresponding to the energy to break (toughness) is calculated as 3.4 kJ·m^{-3} for the EGDE-cross-linked cryogels (Strom et al., 2015), whereas for the cryogels shown in Fig. 7B, it is between 17-75 kJ·m^{-3}, i.e., 5–22 times higher than that of the former cryogels. Fig. 8a showing Young's modulus *E* of the cryogels reveals that *E* increases with increasing DMAA content or methacrylation degree of HA. At Meth = 25% and 5 wt % DMAA, the modulus *E* of freeze-dried cryogels becomes 370 ± 70 kPa which is around 50-fold higher than *E* of dry cryogel formed at 4% Meth and 0.5 wt % DMAA (8 ± 3 kPa, Table S1). Fig. 7 also shows 94–97% compressibility of all cryogels in dry or wet states without any damage. An interesting feature is that the fracture stress σ_f of freeze-dried cryogels increases with increasing DMAA content (left panel in Fig. 8b), whereas a reverse behavior appears for swollen cryogels (right panel). For instance, the maximum fracture stresses σ_f for freeze-dried and swollen cryogels are 3.6 and 2.6 MPa recorded at 5 and 0.5 wt % DMAA, respectively (Fig. 8b, Table S1).

Another characteristic feature is that swollen cryogels with less than 2 wt % DMAA are mechanically stronger than in their dried states. To highlight this behavior, Figs. 9 and S7 compare stress-strain curves of freeze-dried (solid line) and swollen cryogels (dashed curves) below

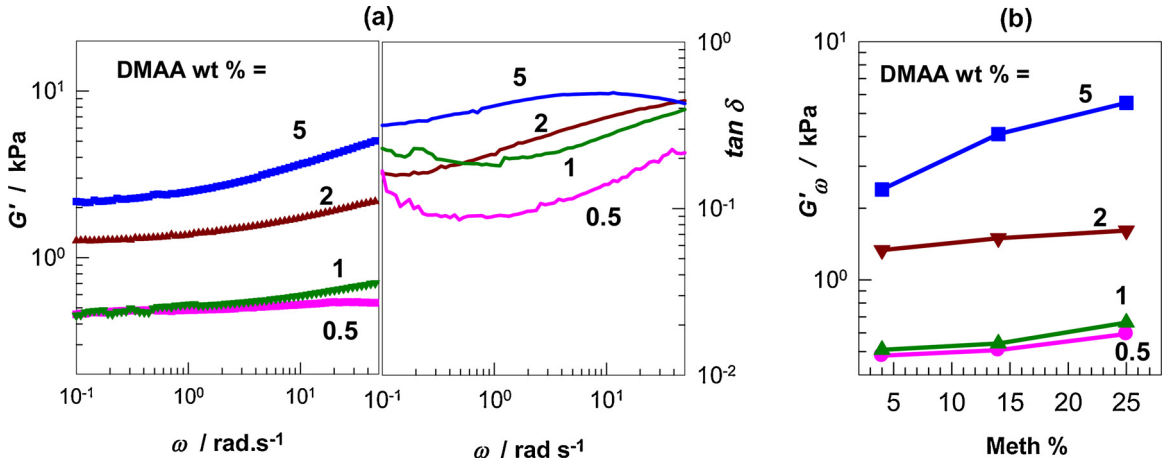

Fig. 6. (a): Frequency dependences of the storage modulus *G'* and loss factor *tan δ* (b) of HA cryogels. Meth = 4%. γ_o = 0.01. DMAA contents are indicated. **(b):** Variation of *G'* at ω = 0.63 rad s^{-1} with the methacrylation degree Meth of HA.

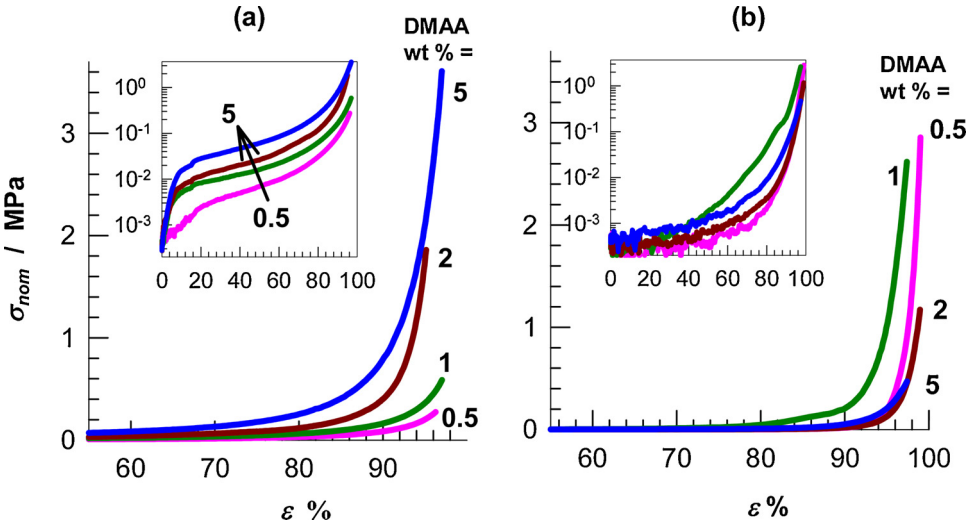

Fig. 7. Stress-strain curves (between 55 and 100% strain) of HA cryogels prepared at various DMAA contents after freeze-drying (a) and after equilibrium swelling in water (b). Meth = 4%. The insets show semi-logarithmic plots over the whole range of strain.

and above 2 wt % DMAA. At 1 wt % DMAA, cryogels in swollen state are around 5-fold stronger than in their dried states, i.e., σ_f = 2.5 vs 0.54 MPa, respectively (Table S1). At 5 wt % DMAA, however, the expected behavior appears in that freeze-dried cryogels are stronger than swollen ones, i.e., σ_f = 3.6 vs 0.49 MPa, respectively. How is it possible that easily squeezable swollen cryogels exhibit higher compressive fracture stress and strain than in their dried states? To explain this observation, we calculated the water content of swollen cryogels depending on the applied strain. At 5 wt % DMAA, water content h_w of hydrated cryogel under 99% compression was 0.18 ± 0.02 whereas at 1 wt % DMAA, h_w under the same compression increased to 0.41 ± 0.03. Previous work shows that at $h_w \leq 0.17$, only bound water exists in hydrated HA and hence, there is no free water molecules acting as plasticizer (Panagopoulou et al., 2013). Thus, higher mechanical strength of swollen HA cryogels formed at a low DMAA content is likely due to the plasticizer effect of free, unbound water improving their large strain properties, which is absent at high DMAA contents.

4. Conclusions

We presented a new cryogelation approach for the fabrication of macroporous HA cryogels with a variety of properties, flow-dependent viscoelasticity, complete squeezability, and a high mechanical strength. HA cryogels were synthesized from 1 wt % methacrylated HA of various methacrylation degrees in aqueous solutions at −18 °C by free-radical mechanism using in situ prepared PDMAA chains as a spacer between 0.5 and 5 wt %. The porous structure of the cryogels investigated by SEM and μ-CT reveals consists of an interconnected open pore structure. It was found that the total open porosity and the average pore diameter decrease from 99 to 90% and from 150 to 90 μm, respectively, with increasing amount of PDMAA. These findings could be explained with the actual concentrations of HA and DMAA as well as the volume of ice during cryogelation. HA cryogels in swollen state sustain up to 2.6 ± 0.2 MPa compressive stress, which is around 2 orders of magnitude higher than those obtained by chemical cross-linking of native HA. This high compressive stiffness originates from the flow of pore water out of the cryogel phase under compression. HA cryogels confined between parallel plates also exhibit reversible strain-dependent apparent gel-to-sol transition behavior due to the flowing-out and flowing-in water through the pores, similar to water squeezing out of a sponge. This flow-dependent viscoelasticity of HA cryogels is similar to that observed with articular cartilage, and produces frictional resistance and hence frictional energy dissipation mechanism in HA cryogels. Such an apparent gel-to-sol transition behavior of HA cryogels is also of great interest in biomaterial and biomedical applications as it protects HA network from damage under large strain conditions and hence act as a self-defense mechanism. It was also found that swollen HA cryogels prepared at a low PDMAA content are mechanically stronger than in

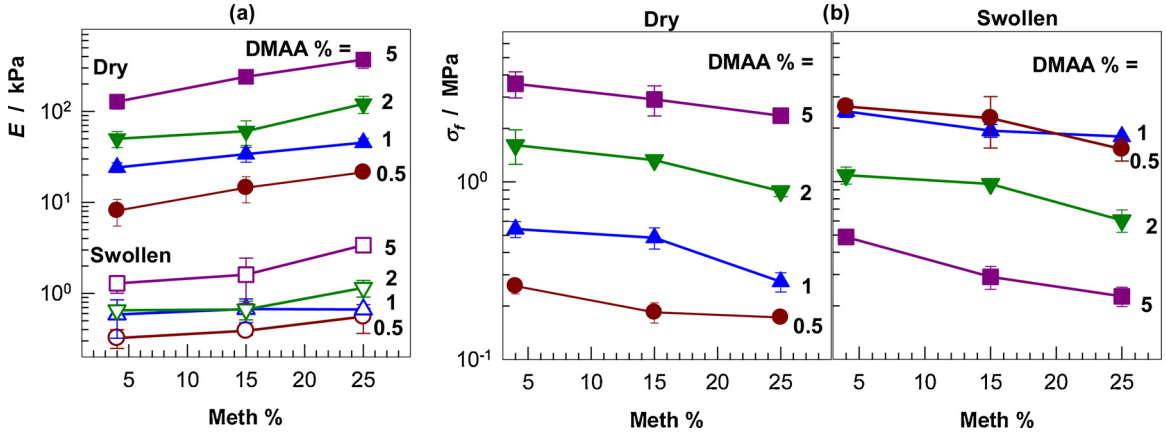

Fig. 8. (a): Young's modulus E of HA cryogels after freeze-drying (filled symbols) and equilibrium swelling in water (open symbols) plotted against Meth %. **(b):** Compressive strength σ_f of freeze-dried (left panel) and swollen HA cryogels (right panel) shown as a function of Meth of HA. DMAA contents indicated.

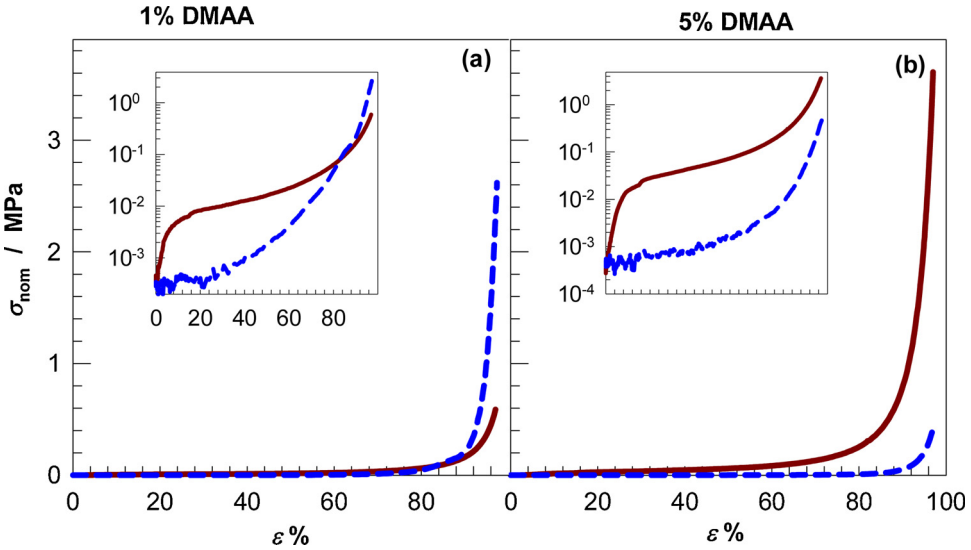

Fig. 9. Stress-strain curves of freeze-dried (solid curve) and swollen cryogels (dashed curve) formed at 1 (a) and 5 wt % DMAA (b). Meth = 4%.

their freeze-dried states, which we attribute to the plasticizer effect of free, unbound water improving their large strain properties.

Acknowledgements

The work was supported by Istanbul Technical University (ITU), BAP39957. The authors would like to thank Dr. Cem Bayram and Dr. H. Evren Cubukcu from Hacettepe University for their assistance in SEM and μ-CT measurements. O.O. thanks the Turkish Academy of Sciences (TUBA) for the partial support.

Appendix A. Supplementary data

Supplementary material related to this article can be found, in the online version, at doi:https://doi.org/10.1016/j.carbpol.2019.115458.

References

Abraham, G. A., de Queiroz, A. A. A., & Roman, J. S. (2001). Hydrophilic hybrid IPNs of segmented polyurethanes and copolymers of vinylpyrrolidone for applications in medicine. *Biomaterials, 22*, 1971–1985.
Ahagon, A., & Gent, A. N. (1975). Threshold fracture energies for elastomers. *Journal of Polymer Science Polymer Physics Edition, 13*, 1903–1911.
Argun, A., Can, V., Altun, U., & Okay, O. (2014). Non-ionic double and triple network hydrogels of high mechanical strength. *Macromolecules, 47*, 6430–6440.
Babic, M., Horak, D., Jendelova, P., Glogarova, K., Herynek, V., Trchova, M., et al. (2009). Poly(N,N-dimethylacrylamide)-coated maghemite nanoparticles for stem cell labeling. *Bioconjugate Chemistry, 20*, 283–294.
Brown, H. R. (2007). A model of the fracture of double network gels. *Macromolecules, 40*, 3815–3918.
Cai, Z., Zhang, F., Wei, Y., & Zhang, H. (2017). Freeze–thaw-induced gelation of hyaluronan: Physical cryostructuration correlated with intermolecular associations and molecular conformation. *Macromolecules, 50*(17), 6647–6658.
Chen, W. Y. J., & Abatangelo, G. (1999). Functions of hyaluronan in wound repair. *Wound Repair and Regeneration, 7*, 79–89.
Collins, M. N., & Birkinshaw, C. (2007). Comparison of the effectiveness of four different crosslinking agents with hyaluronic acid hydrogel films for tissue-culture applications. *Journal of Applied Polymer Science, 104*, 3183–3191.
Collins, M. N., & Birkinshaw, C. (2008). Physical properties of crosslinked hyaluronic acid hydrogels. *Journal of Materials Science Materials in Medicine, 19*, 3335–3343.
Collins, M. N., & Birkinshaw, C. (2013). Hyaluronic acid based scaffolds for tissue engineering – A review. *Carbohydrate Polymers, 92*, 1262–1279.
de Queiroz, A. A. A., Castro, S. C., & Higa, O. Z. (1997). Adsorption of plasma proteins to DMAA hydrogels obtained by ionizing radiation and its relationship with blood compatibility. *Journal of Biomaterials Science, Polymer Edition, 8*, 335–347.
Fraser, J. R. E., Laurent, T. C., & Laurent, U. B. G. (1997). Hyaluronan: Its nature, distribution, functions and turnover. *Journal of Internal Medicine, 242*, 27–33.
Horkay, F., Hecht, A.-M., & Geissler, E. (2006). Similarities between polyelectrolyte gels and biopolymer solutions. *Journal of Polymer Science Part B, Polymer Physics, 44*, 3679–3686.
Hu, Y., & Suo, Z. (2012). Viscoelasticity and poroelasticity in elastomeric gels. *Acta Mechanica Solida Sinica, 25*, 441–458.
Hwang, H.-D., Cho, H.-J., Balakrishnan, P., Chung, C.-W., Yoon, I.-S., Oh, Y.-K., et al. (2012). Cross-linked hyaluronic acid-based flexible cell delivery system: Application for chondrogenic differentiation. *Colloids and Surfaces B: Biointerfaces, 91*, 106–113.
Ibrahim, S., Kothapalli, C. R., Kang, Q. K., & Ramamurthi, A. (2011). Characterization of glycidyl methacrylate – Crosslinked hyaluronan hydrogel scaffolds incorporating elastogenic hyaluronan oligomers. *Acta Biomaterialia, 7*, 653–665.
Kim, H. J., Kim, K. K., Park, I. K., Choi, B. S., Kim, J. H., & Kim, M. S. (2012). Hybrid scaffolds composed of hyaluronic acid and collagen for cartilage regeneration. *Journal of Tissue Engineering and Regenerative Medicine, 9*, 57–62.
Leach, J. B., Bivens, K. A., Patrick, C. W., & Schmidt, C. E. (2003). Photocrosslinked hyaluronic acid hydrogels: Natural, biodegradable tissue engineering scaffolds. *Biotechnology and Bioengineering, 82*, 578–589.
Li, W., Li, J., Gao, J., Li, B., Xia, Y., Meng, Y., et al. (2011). The fine-tuning of thermosensitive and degradable polymer micelles for enhancing intracellular uptake and drug release in tumors. *Biomaterials, 32*, 3832–3844.
Lozinsky, V. I. (2002). Cryogels on the basis of natural and synthetic polymers: Preparation, properties and application. *Russian Chemical Reviews, 71*, 489–511.
Lozinsky, V. I., & Okay, O. (2014). Basic principles of cryotropic gelation. *Advances in Polymer Science, 263*, 49–101.
Lu, X. L., & Mow, V. C. (2008). Biomechanics of articular cartilage and determination of material properties. *Medicine and Science in Sports and Exercise, 40*, 193–199.
Malandrino, A., & Moeendarbary, E. (2019). Poroelasticity of living tissues. In C. Hellmich, D. Mantovani, A. Wong, W. Z. Rymer, & L. Hargrove (Vol. Eds.), *Encyclopedia of biomedical engineering: Vol. 2*, (pp. 238–245). Amsterdam: Elsevier.
Mow, V. C., Kuei, S. C., Lai, W. M., & Armstrong, C. G. (1980). Biphasic creep and stress relaxation of articular cartilage in compression: Theory and experiments. *Journal of Biomechanical Engineering, 102*, 73–84.
Nosellia, G., Lucantonioa, A., McMeeking, R. M., & DeSimonea, A. (2016). Poroelastic toughening in polymer gels: A theoretical and numerical study. *Journal of the Mechanics and Physics of Solids, 94*, 33–46.
Oelschlaeger, C., Bossler, F., & Willenbacher, N. (2016). Synthesis, structural and micromechanical properties of 3D hyaluronic acid-based cryogel scaffolds. *Biomacromolecules, 17*, 580–589.
Okay, O. (2000). Macroporous copolymer networks. *Progress in Polymer Science, 25*, 711–779.
Okay, O., & Lozinsky, V. I. (2014). Synthesis and structure–property relationships of cryogels. *Advances in Polymer Science, 263*, 103–157.
Oyen, M. L. (2014). Mechanical characterisation of hydrogel materials. *International Materials Reviews, 59*, 44–59.
Panagopoulou, A., Molina, J. V., Kyritsis, A., Pradas, M. M., Lluch, A. V., Ferrer, G. G., et al. (2013). Glass transition and water dynamics in hyaluronic acid hydrogels. *Food Biophysics, 8*, 192–202.
Prado, S. S., Weaver, J. M., & Love, B. J. (2011). Gelation of photopolymerized hyaluronic acid grafted with glycidyl methacrylate. *Materials Science and Engineering C, 31*, 1767–1771.
Segura, T., Anderson, B. C., Chung, P. H., Webber, R. E., Shull, K. R., & Shea, L. D. (2005). Crosslinked hyaluronic acid hydrogels: A strategy to functionalize and pattern. *Biomaterials, 26*, 359–371.
Soltz, M. A., & Ateshian, G. A. (1998). Experimental verification and theoretical prediction of cartilage interstitial fluid pressurization at an impermeable contact interface in confined compression. *Journal of Biomechanics, 31*, 927–934.
Strom, A., Larsson, A., & Okay, O. (2015). Preparation and physical properties of hyaluronic acid-based cryogels. *Journal of Applied Polymer Science, 132*, 42194.
Su, E., & Okay, O. (2019). Cryogenic formation-structure-property relationships of poly(2-acrylamido-2-methyl-1-propanesulfonic acid) cryogels. *Polymer, 178*(121603), 1–9.
Tavsanli, B., Can, V., & Okay, O. (2015). Mechanically strong triple network hydrogels

based on hyaluronan and poly(N,N-dimethylacrylamide). *Soft Matter, 11*, 8517–8524.
Tavsanli, B., & Okay, O. (2016). Preparation and fracture process of high strength hyaluronic acid hydrogels cross-linked by ethylene glycol diglycidyl ether. *Reactive & Functional Polymers, 109*, 42–51.
Tavsanli, B., & Okay, O. (2019). Mechanically robust and stretchable silk/hyaluronic acid hydrogels. *Carbohydrate Polymers, 208*, 413–420.
Tomihata, K., & Ikada, Y. (1977). Preparation of cross-linked hyaluronic acid films of low water content. *Biomaterials, 18*, 189–195.
Tuncaboylu, D. C., Sahin, M., Argun, A., Oppermann, W., & Okay, O. (2012). Dynamics and large strain behavior of self-healing hydrogels with and without surfactants. *Macromolecules, 45*, 1991–2000.
Uemura, Y., McNulty, J., & Macdonald, P. M. (1995). Associative behavior and diffusion coefficients of hydrophobically modified poly(N,N-dimethylacrylamides). *Macromolecules, 28*, 4150–4158.
Uzumcu, A. T., Guney, O., & Okay, O. (2018). Highly stretchable DNA/clay hydrogels with self-healing ability. *ACS Applied Materials & Interfaces, 10*, 8296–8306.
Valachova, K., Topolska, D., Mendichi, R., Collins, M. N., Sasinkova, V., & Soltes, L. (2016). Hydrogen peroxide generation by the Weissberger biogenic oxidative system during hyaluronan degradation. *Carbohydrate Polymers, 148*, 189–193.
Wang, F., Yong, X., Deng, J., & Wu, Y. (2018). Poly(N,N-dimethylacrylamide-octadecyl acrylate)-clay hydrogels with high mechanical properties and shape memory ability. *RSC Advances, 8*, 16773–16780.
Weng, L., Gouldstone, A., Wu, Y., & Chen, W. (2008). Mechanically strong double network photocrosslinked hydrogels from N,N-dimethylacrylamide and glycidyl methacrylated hyaluronan. *Biomaterials, 29*, 2153–2163.
Yetiskin, B., & Okay, O. (2019). High-strength and self-recoverable silk fibroin cryogels with anisotropic swelling and mechanical properties. *International Journal of Biological Macromolecules, 122*, 1279–1289.
Zaborina, O. E., Gasanov, R. G., Peregudov, A. S., & Lozinsky, V. I. (2014). Cryostructuring of polymeric systems. 38. The causes of the covalently-crosslinked cryogels formation upon the homopolymerization of N,N-dimethylacrylamide in moderately-frozen aqueous media. *European Polymer Journal, 61*, 226–239.
Zamboni, F., Viera, S., Reis, R. L., Oliveira, J. M., & Collins, M. N. (2018). The potential of hyaluronic acid in immunoprotection and immunomodulation: Chemistry, processing and function. *Progress in Materials Science, 97*, 97–122.